CFD Analysis of Tube-Fin 'No-Frost' Evaporators

Jader R. Barbosa, Jr.
jrb@polo.ufsc.br
Federal University of Santa Catarina
Department of Mechanical Engineering
88040-900 Florianópolis, SC, Brazil

Christian J. L. Hermes
chermes@ufpr.br
Federal University of Paraná
Department of Mechanical Engineering
81531-990 Curitiba, PR, Brazil

Cláudio Melo
melo@polo.ufsc.br
Federal University of Santa Catarina
Department of Mechanical Engineering
88040-900 Florianópolis, SC, Brazil

The purpose of this paper is to assess some aspects of the design of evaporators for household refrigeration appliances using Computational Fluid Dynamics (CFD). The evaporators under study are tube-fin 'no-frost' heat exchangers with forced convection on the air-side and a staggered tube configuration. The calculation methodology was verified against experimental data for the heat transfer rate, thermal conductance and pressure drop obtained for two evaporators with different geometries. The average errors of the heat transfer rate, thermal conductance and pressure drop were 10%, 3% and 11%, respectively. The CFD model was then used to assess the influence of geometric parameters such as the presence and position of the electrical heater coil relative to the tubes, the fin configuration and the width of the by-pass clearance between the outer edge of the fins and the tube bank for conditions typical of the design of household refrigeration appliances
Keywords*: CFD, evaporator, household refrigeration, heat transfer enhancement*

Introduction

Household refrigeration is an essential part of modern life. Recent studies point out that there is approximately one domestic refrigerator for every six people on the planet and that the production of household appliances has doubled over the past twelve years (Coulomb, 2006). Although the energy consumption of a domestic refrigerator or freezer is relatively small compared to other electrical appliances, an increase of just a few percent in the system efficiency represents a significant impact on the overall energy consumption due to the large number of units in operation worldwide.

The main difference between a conventional (or 'static') and a 'no-frost' refrigerator is the type of evaporator used and the associated mode of air flow circulation. In 'no-frost' refrigerators, compartment cooling relies on forced convection heat transfer between the internal air (assisted by a fan) and a tube-fin evaporator (Fig. 1). In conventional refrigerators, plate-tube evaporators (or 'roll-bond' evaporators) are used and the cabinet air circulation is due to natural convection (Hermes et al., 2008).

The majority of the papers on 'no-frost' evaporators deal with the experimental investigation of the air-side heat transfer and pressure drop. Karatas et al. (1996) investigated the effect of non-uniform temperature and velocity distributions of the inlet air flow and concluded that the proposed heat transfer correlation for a uniform distribution of temperature and velocity was equally valid for the non-uniform flow cases. Lee et al. (2002) proposed heat transfer correlations for three different types of 'no-frost' evaporators with distinct fin geometries (discrete flat plate fins, continuous flat plate fins and spine fins). However, no data have been reported on the pressure drop of each evaporator. Melo et al. (2006) carried out *in-situ* tests in an actual refrigerator maintaining all of the original characteristics of the air distribution system. Three evaporators with nearly identical geometric characteristics, but with distinct refrigerant flow arrangements (parallel-flow, counter-flow and 2-pass), were evaluated. As expected, the flow arrangement did not show any effect on heat transfer performance for refrigerant outlet superheating lower than 5°C. However, the counter-flow evaporator exhibited the highest performance at 10°C superheating. Barbosa et al. (2009) investigated the influence of geometric parameters, such as the number of tube rows, fin pitch, number of fins and air flow rate, on the air-side thermal-hydraulic performance of eight tube-fin 'no-frost' evaporator samples. The experimental data was correlated in terms of the Colburn factor, j, and the Darcy friction factor, f, through empirical correlations with ±7% error.

Recently, Computational Fluid Dynamics (CFD) has been employed by several authors to solve the air-side flow and heat transfer in tube-fin heat exchangers (Jang et al., 1996; Atkinson et al., 1998; Leu et al., 2001; Shih, 2003; Perrotin and Clodic, 2004; Zhang, 2005; Erek et al., 2005). Of particular importance to the present analysis is the work of Shih (2003), who carried out a CFD study of the flow distribution and heat transfer in a household refrigeration 'no-frost' evaporator with a non-uniform fin distribution. The effect of the mixing of the air streams drawn from the freezer and fresh food compartments on the temperature and velocity fields have been investigated for a specific condition in which the inlet air velocity was set at 1.26 m/s and the inlet temperatures of the freezer and fresh food compartments were -18 and 3°C, respectively. The temperature of the tube and fins were maintained at -25°C (no account was taken of the fin efficiency) and the presence of the defrosting electrical heaters has not been considered. He identified that the flow mal-distributions were caused by a poor design of the freezer compartment inlet ports and that the stagnation zones within the evaporator severely deteriorated the heat transfer performance of evaporator.

The objective of the present paper is to present a CFD study of the air side flow and heat transfer in a 'no-frost' evaporator under conditions typical of a household refrigerator. In addition to evaluating the effect of the position and diameter of the electrical heater coils on the flow distribution and heat transfer, this study assesses the influence of the by-pass air flow through the side clearances between the outer edge of the fins and the tube bank on the heat transfer rate. A comparison of the CFD calculation predictions with experimental data was performed in order to verify the methodology.

Paper accepted May, 2010. Technical Editor: José A. dos Reis Parise.

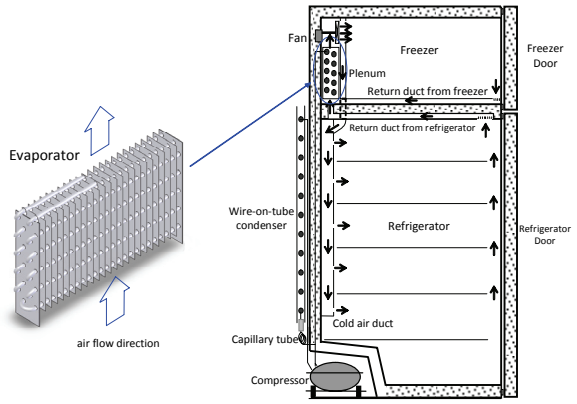

Figure 1. Air flow distribution in a household (top-mount) refrigerator.

Nomenclature

A = *Area, m²*
A_f = *Frontal area, m²*
A_{min} = *Minimum free-flow area, m²*
A_o = *Heat transfer area, m²*
c_p = *Specific heat, J/kgK*
f = *Friction factor*
f_{sg} = *Side-gap flow by-pass fraction*
Fs = *Fin pitch, m*
j = *Colburn j-factor*
k = *Thermal conductivity, W/mK*
m = *Mass, kg*
p = *Pressure, Pa*
$\dot{Q}$ = *Heat transfer rate, W*
T = *Temperature, K*
v = *Velocity, m/s*
V = *Heat exchanger volume, m³*
$\dot{V}$ = *Air flow rate, m³/s*

Greek Symbols

ε = *Dissipation rate of κ, m²/s³*
η_o = *Overall surface efficiency*
κ = *Turbulent kinetic energy, J/kg*
μ = *Viscosity, Pa s*
ρ = *Density, kg/m³*

Subscripts

a air
BL baseline
fin fin
in inlet
out outlet
t turbulent
w water

Computational Modeling

Mathematical Formulation and Implementation

The following assumptions were adopted: (i) steady-state; (ii) Newtonian fluid; (iii) incompressible flow; (iv) constant physical properties; (v) negligible body forces; (vi) no internal heat generation; (vii) turbulent flow; (viii) negligible radiation, viscous dissipation and buoyancy effects; (ix) dry air. In the conservative form, the balance equations for mass, momentum, energy and turbulence quantities become:

$$\nabla \cdot \rho\vec{v} = 0 \tag{1}$$

$$\nabla \cdot \left[\rho\vec{v}\vec{v} - (\mu + \mu_t)\left(\nabla\vec{v} + \nabla\vec{v}^T\right)\right] = -\nabla p \tag{2}$$

$$\nabla \cdot \left[\rho\vec{v}T - \frac{(k + k_t)}{c_p}\nabla T\right] = 0 \tag{3}$$

$$\nabla \cdot \left[\rho\vec{v}\kappa - \left(\mu + \frac{\mu_t}{\sigma_\kappa}\right)\nabla\kappa\right] = G_k + G_b - \rho\varepsilon - Y_m \tag{4}$$

$$\nabla \cdot \left[\rho\vec{v}\varepsilon - \left(\mu + \frac{\mu_t}{\sigma_\varepsilon}\right)\nabla\varepsilon\right] = \rho C_1 S_\varepsilon - \rho C_2 \frac{\varepsilon^2}{\kappa + \sqrt{\nu\varepsilon}} + C_{1\varepsilon}\frac{\varepsilon}{\kappa}C_{3\varepsilon}G_b \tag{5}$$

Equations (4) and (5) are the two-equation Realizable κ-ε Model of Shih et al. (1995). The terms on the right hand side of Eqs. (4) and (5) are due to the production and destruction of κ and ε, and are described in detail in Shih et al. (1995). The turbulent viscosity and thermal conductivity are given by:

$$\mu_t = \rho C_\mu \frac{\kappa^2}{\varepsilon} \tag{6}$$

$$k_t = \frac{c_P \mu_t}{Pr_t} \tag{7}$$

and the default parameters and model constants in Eqs. (4) to (7) have been maintained in the present work. The reason for adopting the Realizable κ-ε Model will be given in the next sub-section.

The governing equations were integrated using a commercial CFD package (Fluent, 2005) which makes use of the Finite Volume Method (Versteeg and Malalasekera, 1995; Maliska, 2004). The momentum and turbulence quantities equations were discretized using the Power Law Scheme and the Second Order Upwind Scheme were used to discretize the mass and energy equations (Versteeg and Malalasekera, 1995). The SIMPLEC model (Van Doormaal and Raithby, 1984) was employed in the pressure-velocity coupling, in which the pressure profile is calculated via the mass conservation equation. The convergence criterion for all balance equations was set at 10^{-4} RMS, the exception being the energy equation for which the convergence criterion was set at 10^{-6} RMS. Convergence tests were performed for the model verification problem (see below). However, tighter criteria did not produce significant improvement in the observed discrepancies in the predictions of the experimental Colburn and friction factors.

Preliminary Model Verification

Before performing the actual simulation of 'no-frost' evaporators, the modeling approach was tested on a well-known compact heat exchanger geometry — surface 8.0 3/8T of Kays and London (1998) — for which experimental data on heat transfer and pressure drop are available. This preliminary analysis is important because it serves as a means of evaluating the appropriateness of boundary and symmetry conditions, interpolation schemes, turbulence models etc. The representative computational cell associated with the 8.0 3/8T surface is shown in Fig. 2. The cell is a 3D grid of approximately 60,000 hexahedrical 8-node elements with boundary conditions prescribed as follows: (i) Uniform velocity and

temperature prescribed at the channel inlet; (ii) Pressure prescribed at the channel outlet; (iii) No-slip and known temperature specified at the tube walls; (iv) Symmetry conditions applied at the mid-tube (symmetry) and mid-channel surfaces; (v) Negligible thermal contact resistance between the fins and the tubes. The 2-D shell conduction model available in the Fluent CFD package was used to calculate the heat transfer in the fin (located at the back *xy* plane). This has proven to be a very good approximation due to the small thickness and high thermal conductivity of the aluminum fin.

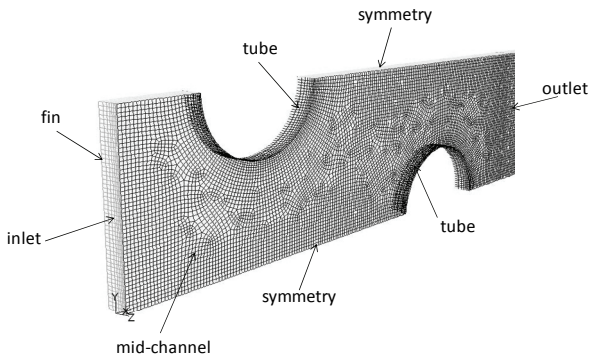

Figure 2. Geometry of the verification case.

Several turbulence models available in the commercial package have been tested and the best results were obtained with the two-equation Realizable κ-ε Model (Shih et al., 1995). The performance of the models was compared for values of Re_{Dh} ranging from 200 to 800. In terms of the Colburn and Fanning factors for heat transfer and pressure drop, the Realizable κ-ε Model predicted the benchmark data with average errors of 3.2% and 7.5% for j and f, respectively.

Modeling of 'No-Frost' Evaporators

Although several geometrical features of 'no-frost' evaporators have been evaluated in the present study, some baseline parameters have been kept approximately uniform in the simulations. The geometry of the baseline evaporator is shown in Fig. 3 with some typical dimensions (Waltrich, 2008).

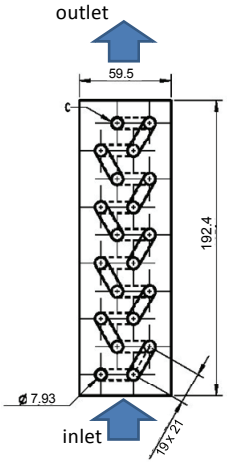

Figure 3. Geometry of the baseline evaporator.

The evaporator width, the tube outside diameter and the fin thickness have been maintained fixed at 307, 7.93 and 0.125 mm, respectively. The fin density was varied according to Table 1, where the values of the heat exchanger geometrical parameters $\sigma = A_{min}/A_f$, $\beta = A_o/V$ and $\gamma = A_{fin}/A_o$ are shown for completeness. In all simulations, the inlet air and the tube wall temperatures were kept at -20 and -33°C, respectively. The air volume flow rate was varied from 34 to 125 m^3/h (1 m^3/h = 3600 m^3/s).

Table 1. Geometric parameters of the simulated evaporators.

Number of fins	Fin density [cm^{-1}]	σ [m^2/m^2]	β [m^2/m^3]	γ [m^2/m^2]
20	0.65	0.721	156.8	0.758
40	1.30	0.708	281.6	0.844
60	1.95	0.698	400.5	0.890

Since a great number of different geometries were simulated, it was quite difficult to perform detailed mesh number and grid independence exercises for all heat exchanger geometries. A typical 3D grid is comprised of around 400,000 control volumes (between approximately 320,000 and 460,000, depending on the number of rows in the heat exchanger). For a given geometry, this number of grid elements was reached after running cases with a progressively more refined mesh until the variation of the calculated heat transfer and pressure drop became less than 2%.

The present calculation methodology has been further tested against experimental data on the heat transfer and air-side pressure drop obtained by Barbosa et al. (2009) for two 'no-frost' evaporator prototypes (samples #3 and #6 of Barbosa et al., 2009). The geometric characteristics of the evaporators are presented in Table 2.

To avoid exceedingly large and therefore unpractical computational times, several simplifications were adopted as far as fin geometry, fin distribution and boundary conditions are concerned. Firstly, it was assumed that the fin surface area was distributed among evenly-spaced identical flat plate continuous fins. As a consequence, in the models, the fin spacing is different than in the real evaporators. However, the finning factor (defined as the ratio of the total external area and the area of the tubes) remains the same and, because of symmetry arguments, solving the fluid flow and heat transfer in half the channel gap between two adjacent fins is assumed enough to represent the overall performance of evaporator. For a more appropriate comparison with the experimental data, the air inlet temperatures were set at 28°C (301 K) for both cases and, for simplicity, it was assumed that the outer wall temperature of the tubes was kept constant at 32°C (305 K). These values are in accordance with the experimental data (Barbosa et al., 2009). It was assumed that the electrical heaters were mounted on the evaporators (and therefore had some effect on the flow field), but were not in operation. The number of mesh volumes employed in the simulation of evaporators #3 and #6 was 344,233 and 416,288, respectively. The boundary conditions for the simulation were specified as in the verification exercise. Thermophysical properties of air and aluminum were assumed constant at 29°C.

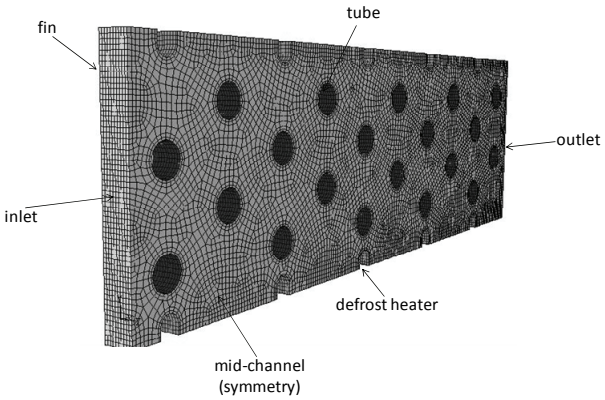

Figure 4. Computational mesh.

Figure 5 presents the fin temperature distribution (5.a), the air temperature (5.b) and the air velocity (5.c) distributions at the channel mid-plane for an overall air volume flow rate of 77 m^3/h (~0.0214 m^3/s); a value which provides a face velocity of approximately 1 m/s. Scales are in K for temperature and m/s for velocity contours, respectively. As can be seen from Fig. 5(a), except for the upper left-hand corner where there is a region of the fin far from any tube and in contact with the cool air, the fin is nearly isothermal. Perhaps, this would not be the case in the real situation where tube-collar thermal contact resistances exist and the fins are discontinuous between two adjacent tubes to facilitate their side mounting on the evaporator coil. In Fig. 5(b), the air temperature increases along the channel and its distribution is approximately symmetrical with respect to the *xz* centre-plane. The air temperature is lower along the by-pass channel between the outer tubes and the electrical resistances, also because of the increased air flow rate along those regions, as can be seen in Fig. 5(c).

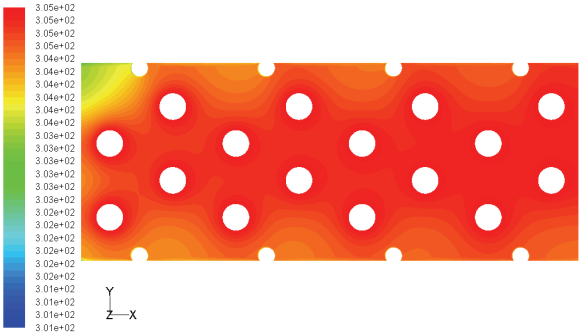

Figure 5. Evaporator #3 (channel mid-plane): (a) Fin temperature distribution, in K; (b) Air temperature distribution in the channel mid-plane, in K; (c) Air velocity distribution, in m/s.

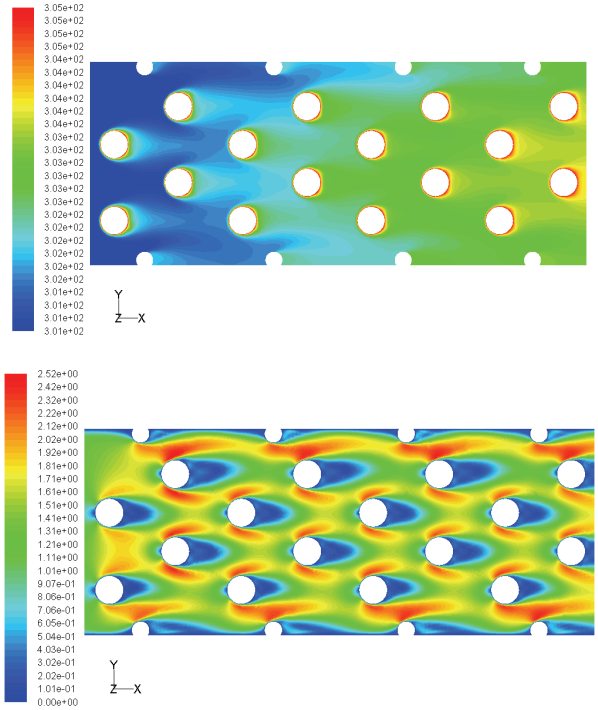

Figure 5. (Continued).

Figure 6 shows a comparison between the experimental and CFD predictions of pressure drop as a function of the air volume flow rate for evaporators #3 and #6. The symbols correspond to the experimental data and the lines to the numerical results. The values of pressure at the evaporator inlet and outlet were calculated through an area average of the local pressure distribution on each section. The agreement is satisfactory, but the numerical results slightly underpredict the experimental data in both cases. The maximum relative error is -20% for evaporator #6. The evaporator heat transfer rate calculated from the numerical simulations is shown in Fig. 7 together with the experimental data. The heat transfer rate was calculated from an energy balance between the air flow inlet and outlet using mass flow averaged temperatures.

Table 2. Geometric parameters of the samples (Barbosa et al., 2009).

Evaporator sample	Tube rows	Length [mm]	Fins	Area [m^2]	Finning factor	Fin density [cm^{-1}]	Mass [g]
#3	8	151	194	fins: 0.61 tube: 0.14 total: 0.75	5.36	1st fin row: 0.79 2nd fin row: 1.00 3rd fin row: 1.97 4th fin row: 1.94	607.1
#6	10	189	261	fins: 0.82 tube: 0.17 total: 0.99	5.82	1st fin row: 0.79 2nd fin row: 1.00 3rd fin row: 1.97 4th fin row: 1.94 5th fin row: 1.97	776.6

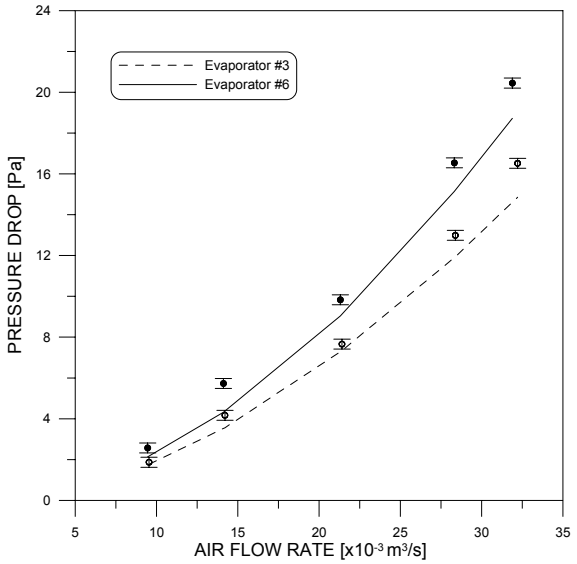

Figure 6. Pressure drop predictions with the numerical model for evaporators #3 and #6 (experimental data of Barbosa et al., 2009).

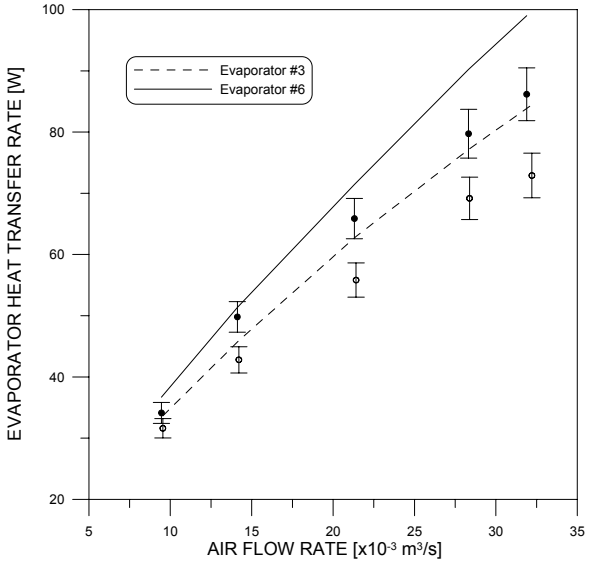

Figure 7. Heat transfer rate predictions with the numerical model for evaporators #3 and #6 (experimental data of Barbosa et al., 2009).

The evaporator heat transfer rate is overpredicted by as much as 15%, by the numerical results at high flow rates. However, the trends are very well picked up by the CFD methodology and, given the many assumptions adopted in the numerical solution, the observed discrepancies can be regarded as acceptable. The air-side thermal conductance, $\eta_o hA$, is shown in Fig. 8. This was calculated based on the ratio of the evaporator heat transfer rate and the logarithmic mean temperature difference estimated from the inlet and outlet mass flow averaged temperatures and the outer tube wall temperature. As can be seen, the agreement between the experimental data and the numerical predictions is quite encouraging, showing that the assumptions that have been adopted can be justified at least for the conditions evaluated here.

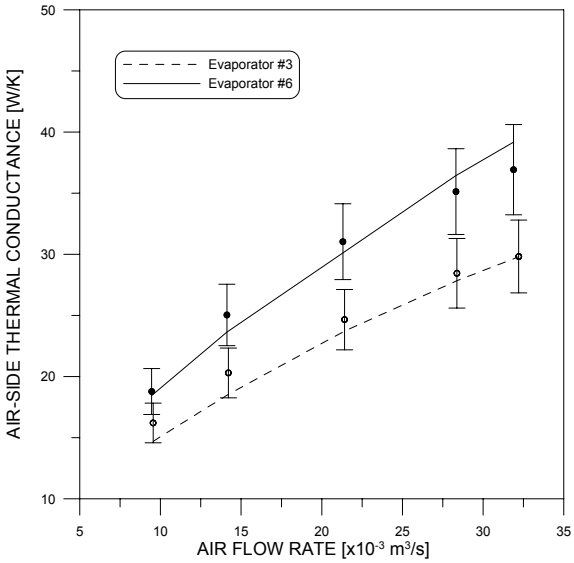

Figure 8. Overall thermal conductance predictions with the numerical model for evaporators #3 and #6 (experimental data of Barbosa et al., 2009).

Numerical Analysis and Discussion of Results

Position of the Electrical Heater Relative to the Tubes

The use of electric heaters is a common feature of the 'no-frost' refrigeration technology. The many types of heaters employed in household evaporators have been reviewed by Kim *et al.* (2006). As can be seen from Fig. 9, the heater employed in the present study is an aluminum sheathed coil (5 mm OD) mounted on the outer edge of the fins, parallel to the tubes. During normal operation of the refrigerator, at pre-determined time intervals, the heater is turned on so as to remove the frost built-up on the surface of the evaporator.

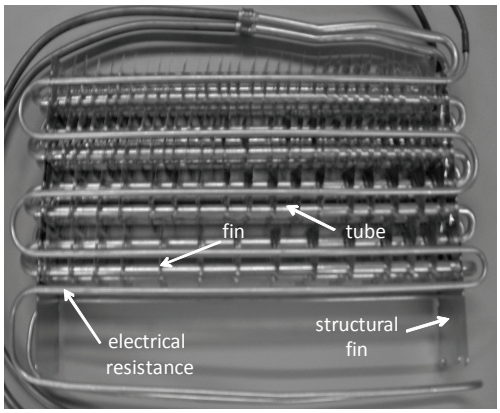

Figure 9. Location of the heaters in a typical 'no-frost' evaporator.

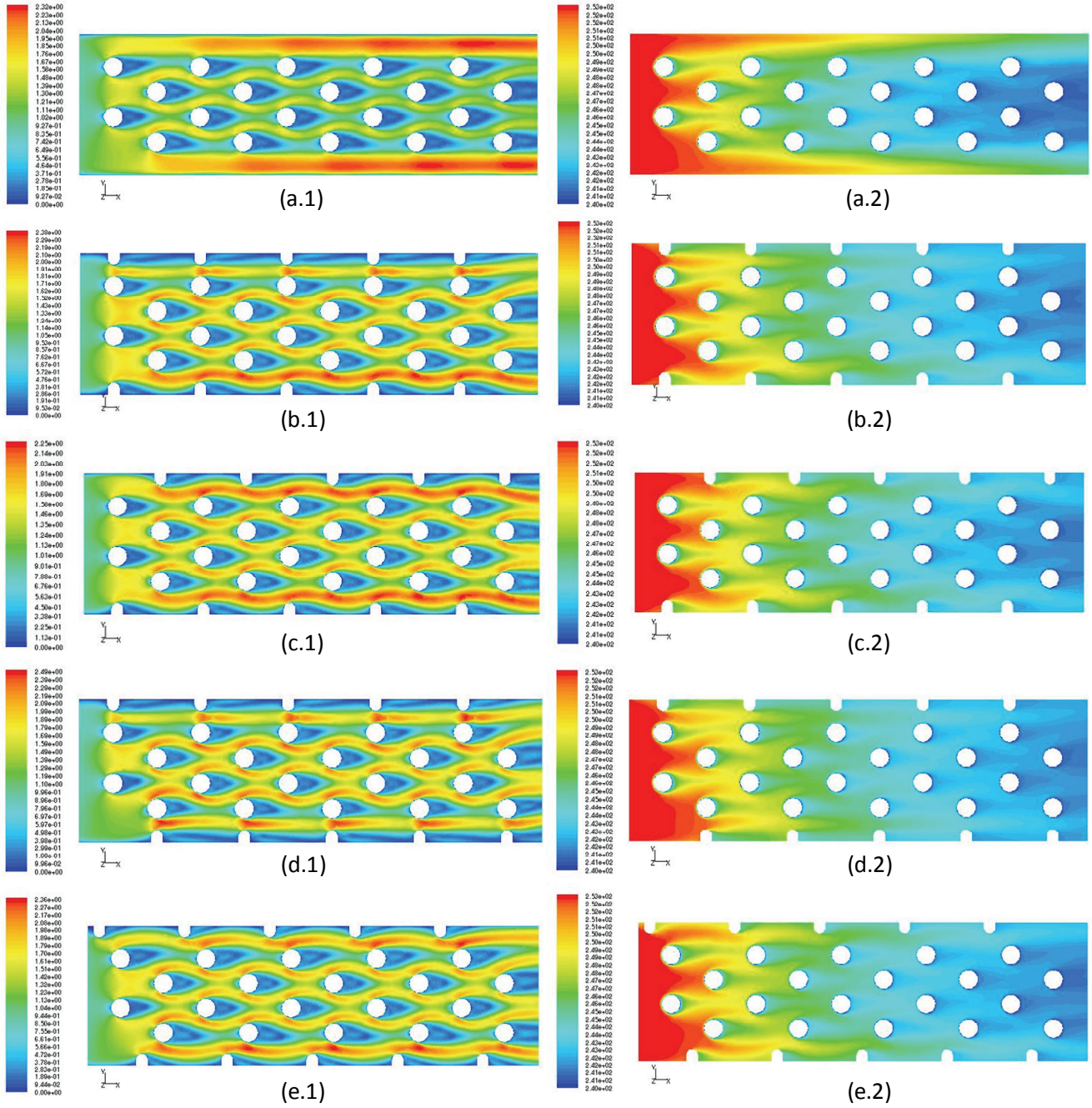

Figure 10. Air flow velocity and temperature (mid-plane) contours for different positions of the electrical heaters relative to the tubes (Conditions of the simulation: Flow rate: 55 m^3/h (~0.0153 m^3/s), fin pitch: 5.55 mm, inlet air temperature: 253K, tube wall temperature: 240K). The figures on the left are velocities, in m/s, and those on the right are temperatures, in K.

Figure 10 illustrates the effect of the position of the electrical heater on the air velocity and temperature (mid-plane). The flow is from left to right and is strongly influenced by the presence of the heaters. In the baseline case (without the heater), a substantial part of the air flow by-passes the tube bank via the side clearances between the outer edge of the fins and the tubes, giving rise to a severe temperature stratification of the air in the y direction. The by-pass fraction is reduced when the heater is mounted on the evaporator, which also causes an increase of the heat transfer rate and the pressure drop between the inlet and outlet. This represents a clear advantage of the aluminum sheathed coil heaters with respect to the other heater types, such as shielded glass tube, metal tube heater, plate heater (Kim et al., 2006). Table 3 shows, for the four different configurations of Fig. 10, the side gap by-pass fraction, f_{sg}, and the heat transfer rate and pressure drop normalized with respect to the baseline configuration. As can be seen, because of the tighter flow restriction between adjacent tube and heater coil, the Aligned configuration (d) presented the lowest by-pass fraction and the highest heat transfer and pressure drop.

The fraction of the total heat transferred through the fins decreases with the by-pass fraction. This is so because relatively more air comes into contact with the primary heat sink (i.e., the tubes) when the heater is present.

Table 3. Geometric configuration of the heaters.

Configuration	$\dot{Q}/\dot{Q}_{BL}$	$\dot{Q}_{fin}/\dot{Q}$	$\Delta p/\Delta p_{BL}$	f_{sg}
Baseline (a)	1	0.818	1	0.574
Staggered (b)	1.108	0.798	1.727	0.468
Half-space (c)	1.100	0.805	1.567	0.387
Aligned (d)	1.118	0.791	1.945	0.371
¼-space (e)	1.102	0.804	1.645	0.474

* based on heater coil diameter (D_c) of 5 mm

The heat transfer as a function of the distance from the inlet was calculated for the baseline case. The evaporator was divided into 5 segments and the heat transfer rate per segment was calculated through an energy balance using the mass flow averaged temperatures at the boundaries of each control volume. The results are shown in Fig. 11 for a typical condition, where the percentage of the total heat transfer rate of the evaporator is shown for each segment. As expected, an exponential decrease of the heat transfer with distance is observed and the last four tube rows (two segments) account for only approximately 18% of the total heat transfer.

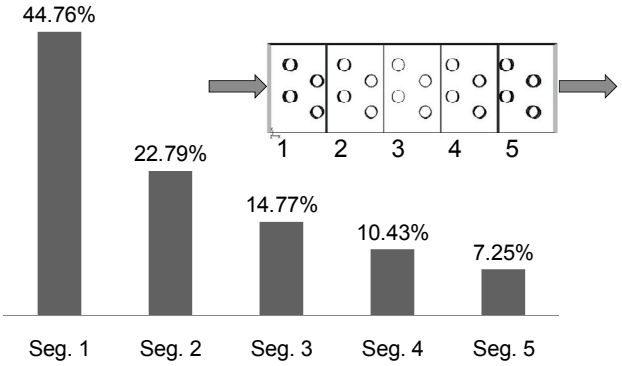

Figure 11. Heat transfer rate per heat exchanger segment (Conditions of the simulation: Flow rate: 55 m^3/h (~0.0153 m^3/s), fin pitch: 5.55 mm, inlet air temperature: 253K, tube wall temperature: 240K).

Table 4 presents an evaluation of the influence of the diameter of the heater coil and of the width of the side gaps. Again, both measures (i.e., increasing the diameter and reducing the clearance) act towards increasing the heat transfer and pressure drop. However, the heat transfer seems to be less sensitive to the geometric changes than the pressure drop, which leads to the conclusion that the Half-Space (D_c = 8 mm) configuration is the most appropriate one due to its lower pressure drop increase with respect to the baseline case.

Fin Geometry

The effect of a different fin configuration on the pressure drop and heat transfer is evaluated in this section. The baseline configuration (continuous fins) is compared with an interrupted fin configuration in which the fins encompass two consecutive tube rows and are offset by $F_s/2$, as shown in Fig. 12. Both fin configurations (continuous and interrupted) are employed in some types of commercially available 'no-frost' evaporators (Lee et al., 2002).

Table 4. Influence of the diameter of the heater coil and of the width of the side gaps.

Configuration	$\dot{Q}/\dot{Q}_{BL}$	$\dot{Q}_{fin}/\dot{Q}$	$\Delta p/\Delta p_{BL}$
Staggered (D_c = 8 mm)	1.130	0.776	2.666
Half-space (D_c = 8 mm)	1.133	0.791	2.186
Aligned (D_c = 8 mm)	1.130	0.762	3.304
¼-space (D_c = 8 mm)	1.138	0.790	2.284
Half-space (D_c = 5 mm/5 mm gap)	1.133	0.768	2.778
¼-space (D_c = 5 mm/5 mm gap)	1.131	0.767	2.771

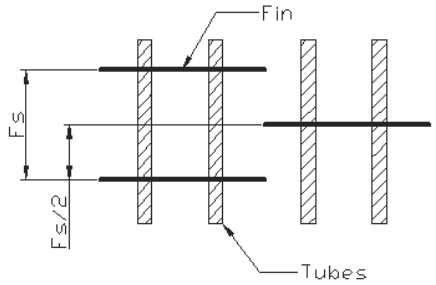

Figure 12. Interrupted fin configuration.

Figure 13 shows the fin temperature distribution for interrupted and continuous fins under identical conditions of air inlet velocity and temperature and tube wall temperature. The average temperature is higher in the interrupted fins, indicating that the heat transfer from the air is more intense than in the continuous fins due to the successive disruption of the boundary layer encountered in the interrupted fin configuration.

A quantitative evaluation of the heat transfer enhancement due to the interrupted fins is presented in Table 5. The heat transfer and pressure drop were calculated as a function the fin type (interrupted – I, continuous – C) and of the fin pitch, and have been normalized with respect to the baseline heat transfer and pressure drop (continuous, F_s = 5.16 mm). The mass of each evaporator (aluminum fins and tubes) and the heat transfer rate per unit mass, both normalized with respect to the baseline, are also presented. As can be seen, for a constant heat transfer area, the interrupted configuration produces an increase in the heat transfer rate of the order of 10%. However, the pressure drop is also increased as a result of the boundary layer disruption due to the offset in the fin distribution between consecutive pairs of tube rows. Since the evaporator pressure drop is small when compared to the overall pressure drop, due to air circulation within the compartments (typically 15% of the total pressure drop), the air flow rate is not much affected by an increase in the air-side pressure drop of the evaporator (Waltrich, 2008).

With a reduction of 33% in the fin surface area and 15% less mass, the evaporator sample with F_s = 7.77 mm and interrupted fins presents a heat transfer rate only 6% lower than the baseline. The pressure drop is 15% less than the baseline, indicating the potential of the application of heat transfer enhancement techniques in 'no-frost' evaporators.

Table 5. Heat transfer enhancement due to the interrupted fins.

F_s [mm]	Fin type	$\dot{Q}/\dot{Q}_{BL}$	$\Delta p/\Delta p_{BL}$	$\left(\frac{\dot{Q}}{m}\right)\Big/\left(\frac{\dot{Q}_{BL}}{m_{BL}}\right)$	m/m_{BL}	Gain (heat transfer)
5.16 (60 fins)	I	1.091	1.105	1.091	1	9%
5.16 (60 fins)	C	1	1	1	1	
7.77 (40 fins)	I	0.940	0.849	1.108	0.850	11%
7.77 (40 fins)	C	0.843	0.796	0.994	0.850	
15.74 (20 fins)	I	0.691	0.667	0.992	0.698	10%
15.74 (20 fins)	C	0.628	0.635	0.902	0.698	
10.41 (30 fins)	I	0.841	0.769	1.090	0.773	—
32.32 (10 fins)	I	0.554	0.595	0.893	0.621	—

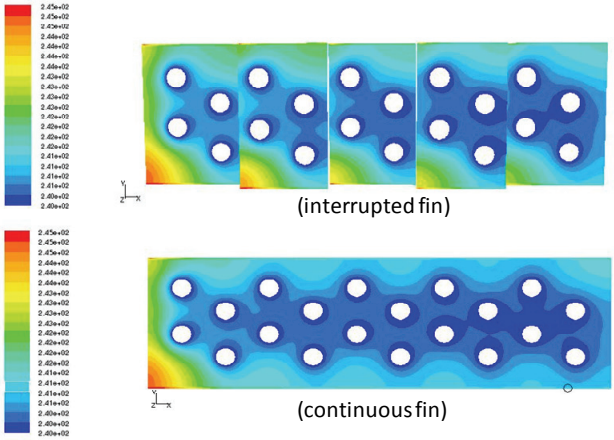

Figure 13. Fin temperature distribution, in K (Conditions of the simulation: Flow rate: 55 m^3/h (~0.0153 m^3/s), fin pitch: 5.55 mm, inlet air temperature: 253K, tube wall temperature: 240K).

Summary and Conclusions

The present paper presented a CFD study of the thermal-hydraulic performance of evaporators for 'no-frost' household refrigeration applications. The methodology was verified against data from the literature (Kays and London, 1998), showing a satisfactory level of agreement for the purpose of engineering calculations. Several important aspects of the air-side heat transfer and pressure drop in 'no-frost' evaporators were identified. These are as follows:

1. The presence and the position of the electrical heater coil relative to the tubes significantly affect the air velocity and temperature distributions, and hence the heat transfer rate, pressure drop, and the fraction of the total air flow rate that by-passes the tube bank through the clearances between the outer edge of the fins and the tubes. The pressure drop and the fraction of the heat transfer removed by the fins are also strongly affected by the diameter of the heater coil and the width of the side clearance.
2. The heat transfer increase associated with the use of interrupted fins has been quantified. A heat transfer rate similar to the baseline configuration (continuous fins) can be achieved with interrupted fins with 33% less fin surface area and an associated air side pressure drop 15% lower than that obtained in the baseline case.
3. The methodology was employed in the prediction of the heat transfer rate, thermal conductance and pressure drop of two 'no-frost' evaporator prototypes, for which experimental data were available (Barbosa et al., 2009). Despite the basic assumptions regarding the evaporator geometry and boundary conditions, the agreement between the predictions of pressure drop, evaporator heat transfer capacity and overall thermal conductance was satisfactory for two evaporator samples with 10 and 8 tube rows. The errors associated with the predictions of heat transfer rate, thermal conductance and pressure drop were 10%, 3% and 11%, respectively.

Acknowledgements

The financial support from Whirlpool S.A. and the Brazilian funding agencies CAPES, CNPq and FINEP is duly acknowledged. The authors are also grateful to Messrs. Guilherme A. Dubiela and Daniel S. Vieira, former students of the Mechanical Engineering Department of the Federal University of Santa Catarina, for their valuable support in the computational work.

References

Atkinson, K.N., Drakulic, R., Heikal, M.R., Cowell, T.A., 1998, "Two and three dimensional numerical models of flow and heat transfer over louvered fin arrays in compact heat exchangers", *International Journal of Heat and Mass Transfer*, Vol. 41, pp. 4063-4080.

Barbosa Jr., J.R., Melo, C., Hermes, C.J.L., 2009, "A study of the air-side heat transfer and pressure drop characteristics of tube-fin 'no-frost' evaporators", *Applied Energy*, Vol. 86, pp. 1484-1491.

Coulomb, D., 2006, "Refrigeration: The challenges associated with sustainable development", Proceedings of the 6th International Conference on Compressors and Coolants, Slovak Republic, CD-ROM

Erek, A., Özerdem, B., Bilir, L., İlken, Z., 2005, "Effect of geometrical parameters on heat transfer and pressure drop characteristics of plate fin and tube heat exchangers", *Applied Thermal Engineering*, Vol. 25, pp. 2421-2431.

FLUENT 6.2, 2005, User Manual, Fluent Inc.

Hermes, C.J.L., Melo, C., Negrão, C.O.R., 2008, "A numerical simulation model for plate-type, roll-bond evaporators", *International Journal of Refrigeration*, Vol. 31, pp. 335-347.

Jang, J.Y, Wu, M.C., Chang, W. J., 1996, "Numerical and experimental studies of three-dimensional plate fin and tube heat exchangers", *International Journal of Heat and Mass Transfer*, Vol. 39, pp. 3057-3066.

Karatas, H., Dirik, E., Derbentil, T., 1996, "An experimental study of air-side heat transfer and friction factor correlations on domestic refrigerator finned-tube evaporator coils", Proceedings of the 8th International Refrigeration and Air Conditioning Conference at Purdue, West Lafayette, IN, July 25-28.

Kays, W.M., London, A.L., 1998, "Compact Heat Exchangers", 3rd Ed., Krieger, Malabar, FL. 335 p.

Kim, Y., Tikhonov, A., Shin, Y., Lee, J., 2006, "Experimental study on high performance defrosting heater for household refrigerator", Proceedings of the 13th International Heat Transfer Conference, Sydney, Australia, August 13-18.

Lee, T.-H., Lee, J.-S., Oh, S.-Y., Lee, M.-Y., Lee, K.-S., 2002, "Comparison of air-side heat transfer coefficients of several types of evaporators of household freezer/refrigerators", Proceedings of the 9th International Refrigeration and Air Conditioning Conference at Purdue, West Lafayette, IN, July 16-19.

Leu, J.S., Liu, M.S., Liaw, J.S., Wang, C.C., 2001, "A numerical investigation of louvered fin-and-tube heat exchangers having circular and oval tube configurations", *International Journal of Heat and Mass Transfer*, Vol. 44, pp. 4235-4243.

Maliska, C.R., 2004, "Transferência de calor e mecânica dos fluidos computacional", 2nd Ed., LTC, Rio de Janeiro, RJ, 472 p.

Melo, C., Piucco, R.O., Duarte, P.O.O., 2006, "In-situ performance evaluation of no-frost evaporators", Proceedings of the 11th International Refrigeration and Air Conditioning Conference at Purdue, West Lafayette, IN, July 17-20.

Perrotin, T., Clodic, D., 2004, "Thermal-hydraulic CFD study in louvered fin-and-flat-tube heat exchangers", *International Journal of Refrigeration*, Vol. 27, pp. 422-432

Shih, T.-H., Liou, W.W., Shabbir, A., Yang, Z. and Zhu, J, 1995, "A new eddy-viscosity model for high Reynolds number turbulent flows – Model development and validation", *Computers and Fluids*, Vol. 24, pp. 227-238.

Shih, Y.C., 2003, "Numerical study of heat transfer performance on the air side of evaporator for a domestic refrigerator", *Numerical Heat Transfer*, Part A, Vol. 44, pp. 851-870.

Van Doormaal, J.P. and Raithby, G.D., 1984, "Enhancements of the SIMPLE method for predicting incompressible fluid flows", *Numerical Heat Transfer*, Vol. 7, pp. 147-163.

Versteeg, H.K., Malalasekera, W., 1995, "An Introduction to Computational Fluid Dynamics: The Finite Volume Method", Pearson Prentice-Hall, 257 p.

Waltrich, P.J., 2008, "Analysis and Optimization of Accelerated Flow Evaporators for Household Refrigeration Applications" (in Portuguese), MSc thesis, Federal University of Santa Catarina, Florianópolis, SC, Brazil.

Zhang, J., 2005, "Numerical Simulations of Steady Low-Reynolds Number Flows and Enhanced Heat Transfer in Wavy Plate-Fin Passages", PhD. thesis, University of Cincinnati, OH, USA.